Journal of Engineering Science and Technology
Vol. 12, No. 10 (2017) 2805 - 2825

NUMERICAL AND EXPERIMENTAL INVESTIGATION ON THE FLUTTER OF CANTILEVERED PLATES WITH FREE LEADING EDGE IN AXIAL FLOW

I. P. G. SOPAN RAHTIKA[1, 2, *], I. N. G. WARDANA[2], A. A. SONIEF[2], E. SISWANTO[2]

[1]Department of Mechanical Engineering, Bali State Polytechnics, Bukit Jimbaran, Kuta Selatan, Badung, Bali, Indonesia
[2]Department of Mechanical Engineering, Brawijaya University, Jalan M.T. Haryono, No. 109, Malang, East Java, Indonesia
*Corresponding Author: sopan_rahtika@yahoo.com

Abstract

This paper reports the results of the numerical and experimental investigation on the flutter of cantilevered thin flat plates with free leading edge in axial flow. Three methods of *in-vacuo* modal analyses of the plates are presented and compared in this paper, namely the finite element modal analysis using ANSYS STUDENT Modal, the analytical beam model, and the experimental modal analysis. In this study, the numerical Fluid Structure Interaction was performed using the ANSYS STUDENT Structural Transient Analysis and ANSYS STUDENT CFX to obtain the system response in the time domain. Furthermore, the experimental investigation was conducted in the smooth flow of a wind tunnel to observe the flutter speeds of the plates and their vibration characteristics. The plates' vibration behaviors were mapped on the normalized air speed. The normalized air speed can be divided into four speed zones based on the experimental plates' vibration characteristics. A new finding observed during the experiments is the presence of intermittent vibration behavior that is unique to the free leading edge configuration and has not been reported by other researchers in the earlier references of the clamped leading edge configuration. The potential application of this Fluid Structure Interaction configuration to wind harvesting is inquired.

Keywords: Cantilevered plate, Free leading edge, Axial flow, Flow-induced flutter, Intermittent vibration.

Nomenclatures

A	Cross-section of the plate, m^2
b	Plate thickness, m
C	Structural global damping matrix
c	The ratio of beam elasticity to its inertia
C_a	Aerodynamic damping matrix
dy/dt	Velocity of the tip of the free leading edge of the plate (first derivative of y with respect to t), m/s
E	Young modulus of elasticity, Pa
F_a	Aerodynamic force vector
h	Plate width, m
I	Second moment of area $I = bh^3/12$, m^4
K	Structural global stiffness matrix
K_a	Aerodynamic stiffness matrix
k_{eq}	Equivalent structural stiffness, N/m
L	Plate length, m
M	Structural global mass matrix
m_{eq}	Equivalent structural mass, kg
n	Indices for mode shape number
t	Time, s
U	Displacement vector of the plate's elements, m
$\dot{U}$	Velocity vector of the plate's elements, m/s
$\ddot{U}$	Acceleration vector of the plate's elements, m/s^2
V	Air speed, m/s
V_f	Plate flutter speed, m/s
V_{norm}	Normalized speed
W	Beam deflection, m
x	Distance to the clamped side, m
X	Spatial solution of w, m
y	Displacement of the tip of the free leading edge of the plate, m
$\dot{y}$	Velocity of the tip of the free leading edge of the plate, m/s
$\ddot{y}$	Acceleration of the tip of the free leading edge of the plate, m/s^2
Y	Normalized displacement of tip the free leading edge of the plate

Greek Symbols

σ	Constant for the mode shape coefficient $\frac{\sinh \beta_n l - \sin \beta_n l}{\cosh \beta_n l + \cos \beta_n l}$
β	$\beta^4 = \rho A \omega / EI$
ρ	Mass density of the plate, kg/m^3
ω	Natural frequency, rad/s

Abbreviations

CFD	Computational Fluid Dynamics
FSI	Fluid Structure Interaction
LCO	Limit Cycle Oscillation

1. Introduction

There have been a vast number of works on the flutter of thin flat plates which has become a more extensive research topic in recent years. Despite the simplicity of the configuration and the ease of fabricating the experimental apparatus of these setups, the scientific phenomena behind them are still very complex. Due to the current global energy scarcity issue, there are new research trends in utilizing this configuration to harvest energy from the wind.

The development of the applications of the thin flat plates towards wind harvesting has expanded these research areas to seek a better configuration to obtain more effective and efficient conversion of energy. The utilization of thin flexible plates for wind energy harvesting motivated Deivasigani et al. [1] to examine the flutter characteristics of interconnected beams with various hinge positions. With similar motivation, this paper extends the search towards a new free leading edge axial flow configuration. This configuration is anticipated to be more suitable for low wind speed energy harvesting compared to the fixed leading edge configuration since the flutter occurs at the first mode shape instead of the second.

The history of flutter can be traced to the earliest seminal theoretical work done by Rayleigh [2] on the instability of an elastic plate of infinite dimension immersed in axial flow. A more practical scientific understanding of the flutter phenomenon can be found in NACA Technical Report No. 496 on the General Theory of aerodynamic instability and the Mechanism of Flutter [3]. In that report, Theodorsen theoretically explained how flutter can occur on the aircraft wings as a result of the interaction between the elastic, inertia, and aerodynamic forces. In that report, the dynamics of the aircraft wings was mathematically modeled to explain the flutter mechanism. That research was continued into the experimental investigation and reported in NACA Technical Report No. 685 [4]. Later, the effect of aerodynamic balance and the effect of adding a tab to the aileron were reported in NACA Technical Report 736 [5].

The advancement of the printing industry that demanded a higher speed machine motivated Watanabe et al. [6] to investigate paper flutter problems. Both the potential flow and numerical Navier-Stokes methods were used to explain paper flutter mode shape as a function of mass ratio in their investigation. They also executed time marching analysis using a Navier-Stokes code. Experimentally Watanabe et al. [7] observed the air speed limit required for the paper to stop fluttering.

The Fluid Structure Interaction (FSI) of a flag or a long ribbon shares a lot of similarity with that of a thin flat plate. Studies of flags and ribbons have been done by Connel and Yue [8], Lemaitre et al. [9], Michelin et al. [10], Manela and Howe [11], and Virot et al. [12].

Several recent studies of thin flat plates have been done by Gibbs et al. [13], Tang and Dowell [14], Tang et al. [15], Tang and Païdoussis [16], Zhao et al. [17], Howell et al. [18, 19], Doaré et al. [20], Huang and Zhang [21]. The work of Tang and Dowell [14] was about nonlinear flutter and Limit Cycle Oscillation (LCO) of two-dimensional panels in low subsonic flow, and later was extended to three-dimensional panels by Tang et al. [15].

Gibbs et al. [13] performed experimental and theoretical work on the flutter of a flat plate with a fixed leading edge using the three-dimensional vortex-lattice method. Gibbs' report comprehensively described the characteristics of plate

flutter as a function of the mass ratio and the aspect ratio. Tang and Païdoussis [16] discussed the flutter of two flat plates which were positioned in parallel with the axial direction of the fluid flow. The dynamics of the system was built to produce nonlinear models. Zhao et al. [17] discussed both theory and experiment of the flutter of a flat plate. The discussion emphasizes nonlinear analysis to produce of the Poincaré maps. The nonlinear analysis results were compared to experimental results. Howell et al. [18] used fluid-flow interactions to discuss the nature of a cantilevered plate with ideal flow. Their work was continued to include the effect of inertial homogeneity to the flutter [19]. Huang and Zhang [21] executed a coupled modal analysis using the full Theodorsen airfoil theory within the linear framework.

Eloy et al. [22] developed a theoretical model that enabled the prediction of flutter modes, their frequencies, and growth rates using the Galerkin method and Fourier transforms. The aeroelastic instability of a flexible plate has been investigated using weakly nonlinear analyses by Eloy et al. [23]. Later, a deeper investigation was focused on the origin of the instability hysteresis [24].

The phenomenon of bimodal flutter was found by Drazumeric et al. [25] in a flexibly mounted rigid airfoil with a flexible plate attached to its trailing edge. The flutter behavior was predicted using the *eigenfunction* expansion approach and bimodal flutter behavior was indicated in the experimental investigation.

Flutter in human biological systems has been investigated by Balint and Lucey [26], Huang [27], and Howell et al. [18]. They explained that snoring phenomena are similar to the flutter of a cantilevered flexible plate in axial flow. The utilization of flutter phenomena for wind energy harvesting has been explored by Doaré et al. [28] and Dunmon et al. [29]. The other works on energy harvesting using a slender structure in the wake of a bluff body were also conducted by Allen and Smits [30] and Kuhl and DesJardin [31].

Due to their complexities, flutter phenomena of plates have continued to be investigated over the last two years. Howell and Lucey [32] explored spring-mounted plate flutter in uniform flow. Flutter prediction of supersonic cantilevered plates was observed by Meijer et al. [33]. More recent studies on plate flutter were also done by Fernandes and Mirzaeisefat [34], Cunha-Filho et al. [35], Darbandi and Fouladi [36], and Tubaldi et al. [37].

A computational study of the free leading edge with the presence of a bluff body was conducted by Akaydin et al. [38] with assumed mode shapes. Their work was focused on utilizing this extraneously induced excitation system for energy harvesting. In contrast to Akaydin's work, the present study is focused on the aeroelastic FSI behavior of the fixed trailing edge cantilevered plate in smooth air flow without the bluff body.

In this paper, the *in-vacuo* structural modal analysis is presented in three different ways, namely an analytical method using the beam approximation, a three-dimensional finite element modal analysis using ANSYS STUDENT Modal, and an experimental modal analysis using a high-speed camera. The nature of the air flow surrounding the plate is presented as the result of the numerical FSI analysis using ANSYS STUDENT Structural Transient Analysis and ANSYS STUDENT CFX. The results of the experimental FSI of the plates are also presented in the form of a mapping of the air-speed zones based on the

plates' vibration characteristics, the phase plane of the oscillation of the tip of the plates, and the flutter speed as a function of plate thickness for various plate sizes. Since this investigation is motivated by the desire to explore a new configuration that is more suitable for low-speed wind harvesting, an assessment of this study in respect of electrical energy conversion is also in the discussion section. The relevance of this study in complementing previous research by explaining the snoring mechanism is also discussed at the end of the paper.

2. Theory of Flat Plate Flutter

Aeroelasticity is the science which deals with the interactions between the forces of inertia, elasticity, and aerodynamics on a structure. Aeroelasticity is divided into two, namely static and dynamic aeroelasticity. Static aeroelasticity is about the interaction between aerodynamic forces and elastic forces on a structure, while the dynamic aeroelasticity is about the interaction of those two types of forces plus the inertia forces.

Flutter is a dynamic aeroelastic phenomenon that is potentially damaging where aerodynamic forces work together with the natural modes of vibration of a structure to produce an unstable periodic motion. Aerodynamic force serves as an input vibration-energy to the structure. If the amplitude of the vibration is not damped by the system's damping, it will increase in size and will eventually lead to structural failure. In spite of its destructive potential, a structure that inherits flutter characteristic promises an advantage as an energy conversion tool in its subcritical or post-critical state.

The schematic of the system that was investigated is shown in Fig. 1. The plate was clamped at its downstream end and left free at its leading edge. Like other cases in dynamic aeroelastic phenomena, the numerical governing equation of motion of the cantilevered plate subjected to counter axial flow can be expressed as

$$M\ddot{U} + C\dot{U} + KU = F_a \tag{1}$$

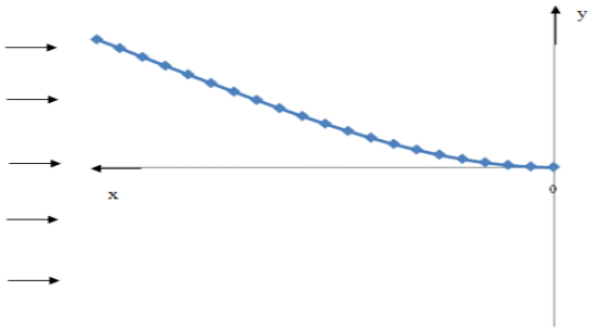

Fig. 1. Schematic showing the parameters of interest for the theoretical analysis.

Equation (1) is the full plate's aeroelastic equation of motion which is the plate's structural dynamics subjected to aerodynamic force F_a which value is a function of the plate's movement. When F_a is set to zero, the above equation becomes the plate's *in-vacuo* equation of motion. The *eigenvalue* analysis on this *in-vacuo* equation of motion will give the plate's mode shapes and their corresponding natural frequencies.

The aerodynamic force F_a is nonlinear in nature. For the purpose of predicting the flutter speed, F_a is often linearized to be

$$F_a = C_a\dot{U} + K_aU \tag{2}$$

Substituting the linearized F_a into the full plate's aeroelastic equation of motion yields the plate's linearized equation of motion:

$$M\ddot{U}+(C-C_a)\dot{U}+(K-K_a)U = 0 \tag{3}$$

The *eigenvalue* analysis of this linearized equation will give the value of the flutter speed of the plate. Numerous studies (i.e. Tang et al. [15], Watanabe et al., [6], Huang [27], Gibbs et al. [13]) have used a linearized aeroelastic equation to predict the flutter speed with different methods for evaluating the aerodynamic force, F_a. The present study does not used *eigenvalue* analysis. Instead, it simulates the plate's aeroelastic equation of motion, Eq. (1) in a time domain. The plate's dynamic response is calculated at every time step using ANSYS Structural Transient Analysis with the adjusted value of F_a that is calculated using ANSYS STUDENT CFX.

If the damping forces are ignored, the above equation becomes

$$M\ddot{U}+(K-K_a)U = 0 \tag{4}$$

It is reasonable to simplify the system being investigated to a one degree of freedom system since the experiments showed that the dominant mode shape that appeared was the first mode shape. If the variable of choice to represent the system is the deflection of the tip of the leading edge of the plate (y) the simplified one degree of freedom system becomes

$$m_{eq}\ddot{y}+k_{eq}y=F_a \tag{5}$$

The simplified one degree of freedom model is useful in understanding the bistable nature of the free leading edge axial flow plate configuration by means of static aeroelasticity analysis. When the air flow is set to zero, the system has only one stable equilibrium position, which is y=0. As the air flow increases, the value of F_a also increases and tends to move the plate away from the original equilibrium position. Two new stable equilibrium positions (y_{equi}) will be introduced to the system as the air flow increases with values

$$k_{eq}y_{equi} = F_a \tag{6}$$

and the original equilibrium position y=0 becomes unstable. This intrinsic bistable nature of the free leading edge configuration is very useful in explaining the phenomenon of intermittent vibration in the later section.

3. Numerical Investigation

It is a standard procedure in flutter analysis to perform structural modal analysis before doing theoretical and experimental FSI analysis. Structural modal analysis provides the potential choices regarding on which mode the flutter will occur. Not all mode shapes obtained from *in-vacuo* structural analysis will experience flutter in any specific FSI configuration. Stability of each mode shape is an object of the FSI analysis, and it can be determined by means of numerical or experimental methods. In this study, three ways of *in-vacuo* modal analyses were performed and compared.

3.1. Governing structural equation using Euler-Bernoulli beam approximation

The first modal analysis performed was an analytical method using the beam approximation, the second was a three-dimensional finite element analysis using ANSYS STUDENT Modal analysis, and the third was experimental modal analysis using a high-speed camera. In this section, the analytical approach to modal analysis using the flexible beam model will be discussed. The analysis starts by modeling the beam through a cantilevered beam governing equation:

$$\frac{\partial^2 w(x,t)}{\partial t^2} + c^2 \frac{\partial^4 w(x,t)}{\partial x^4} = 0 \tag{7}$$

with

$$c = \sqrt{\frac{EI}{\rho A}} \tag{8}$$

The thin plate can be modeled as a clamp-free plate. The mode shape of a plate based on the distributed parameter beam [39] is

$$X(x) = \cosh(\beta_n x) - \cos(\beta_n x) - \sigma_n(\sinh(\beta_n x) - \sin(\beta_n x)) \tag{9}$$

where for n=1 then $\beta_n L$=1.8751 and σ_n =0.7341
n=2 then $\beta_n L$=4.6941 and σ_n =1.0185
n=3 then $\beta_n L$=7.8548 and σ_n =0.9992
n=4 then $\beta_n L$=10.9955 and σ_n =1.0000
n=5 then $\beta_n L$=14.1372 and σ_n =1.0000
n=6 then $\beta_n L$=17.2788 and σ_n =1.0000

The results of modal analysis of five plates are presented in this paper. Five specimens that were observed for modal analysis were copper plates (Young's modulus of elasticity of 110 GPa, mass density of 8960 kg/m^3, and Poisson ratio of 0.34) with an aspect ratio of 1:6 and three values of thickness of 60, 80, and 130 microns. The plates with thicknesses of 60 and 80 microns have dimensions of 1 cm × 6 cm and 1.5 cm × 9 cm. The plate with a thickness of 130 microns has dimensions of 1.5 cm × 9 cm. Note that the plate with a thickness of 130 microns and dimensions of 1 cm × 6 cm was later excluded from the observations since during the FSI analysis it was found to have a flutter speed higher than the maximum wind tunnel speed being used. The results of the analysis based on the

above beam model are shown side by side with the results of the three-dimensional finite element model in Fig. 2.

The natural frequency of a clamped-free beam [39] can be obtained based on the following formula

$$\beta^4 = \frac{\rho A \omega^2}{EI} \tag{10}$$

The natural frequencies calculated based on the beam model are presented on Table 1 and compared with the results of numerical and experimental analyses.

Table 1. The comparison of the result of the modal analysis with three different methods.

Plate dimension	Analytical (Hz)	E×perimental (Hz)	Numerical (Hz)
60 microns × 1 cm × 6 cm	9.43	9.13	9.69
80 microns × 1 cm × 6 cm	12.58	11.05	12.83
60 microns ×1.5 cm × 9cm	4.19	4.04	4.75
80 microns × 1.5 cm × 9 cm	5.59	5.38	6.37
130 microns × 1.5 cm × 9 cm	9.08	7. 78	9.25

3.2. Three-dimensional structural modal analysis

Analytical modal analysis using the beam approach has the advantage of simplicity. Three-dimensional numerical analysis is more complex but can show more complete mode shape behavioral tendencies that can be demonstrated with a cantilevered plate in all dimensions. Modal analysis of a cantilevered flat plate was conducted using ANSYS Modal to obtain the natural frequencies and the corresponding mode shape.

Structural analysis is usually used to predict the mode shapes prior to FSI. The beam approximation method has been widely used in the structural section of flutter analysis of cantilevered plates in axial flow. Gibbs et al. [13] used the beam approximation to analyze the mode shapes of cantilevered aluminum plates and Deivasigani et al. [1] used it to analyze the mode shape of polypropylene plates.

Comparing the analytical beam model with the three-dimensional finite element method has the purpose of providing a theoretical proof that the use of the beam model is valid to represent a dynamic plate in an axial flow configuration. As shown in Fig. 2, the two methods agree with one another up to the second mode shape. The difference occurs on the third mode shape. The third mode shape from the three-dimensional analysis is a twisting mode. Due to the nature of the one-dimensional analysis, the twisting mode does not appear in the beam model.

Earlier experimental flutter work on the axial flow configuration with a fixed leading edge by other researchers (e.g. Deivasigani et al. [1] and Huang [27]) showed that the first mode shape is stable because the airflow will strengthen the rigidity of the plate and flutter will occur in the second mode shape. Since flutter occurs in the second mode shape for a fixed leading axial flow plate and the twisting mode appears in the third mode of the three-dimensional analysis, it is adequate to use the beam model to do subcritical and flutter analyses for such a configuration.

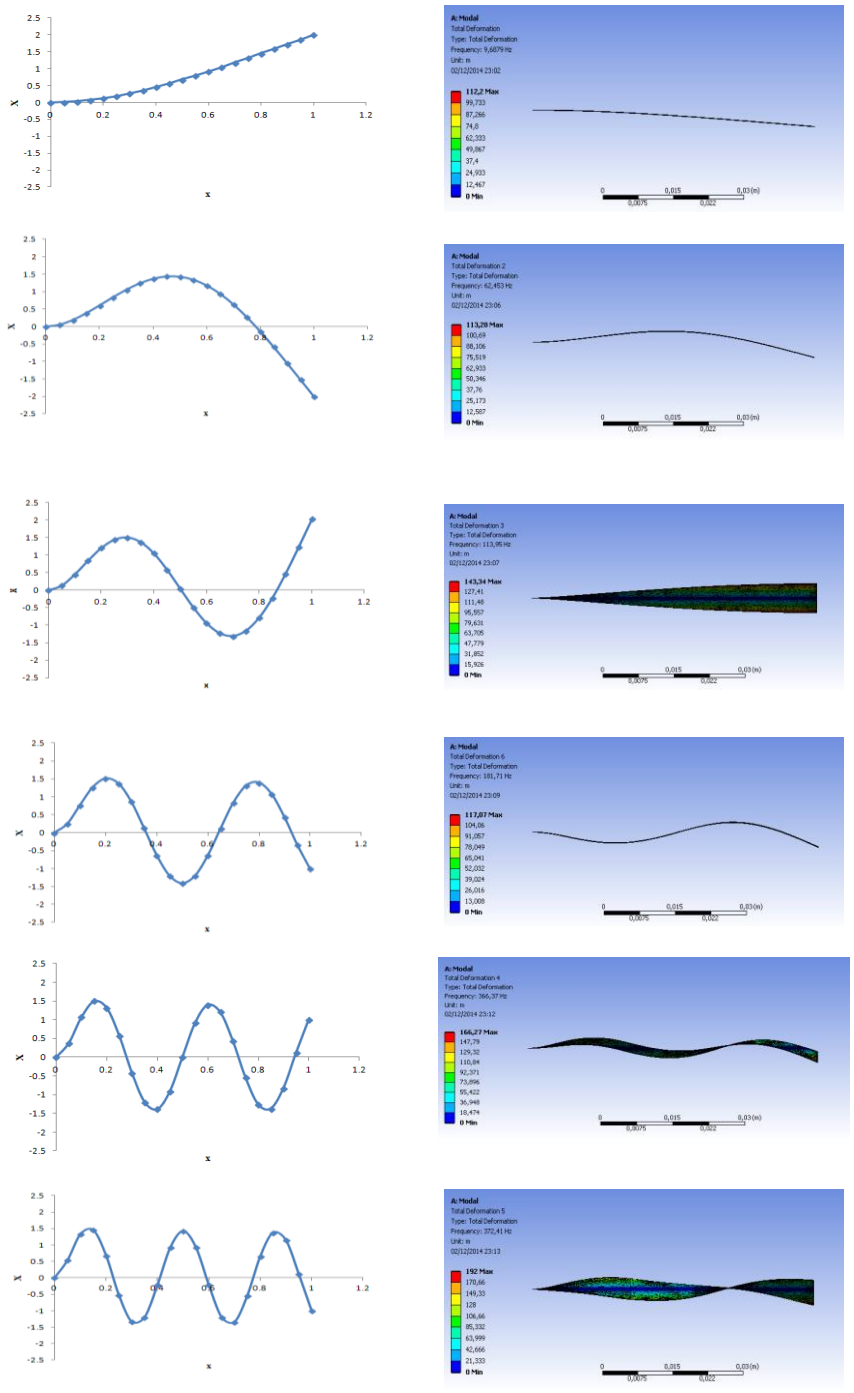

(a) **(b)**

Fig. 2. (a) The first six plate mode shapes based on the analytical beam model approach, (b) The first six plate mode shapes based on the three dimensional finite element analysis using ANSYS STUDENT Modal.

A similar case is also applicable to the free leading-edge configuration. As will be discussed in more detail later in the FSI section, flutter will occur in the first mode shape in the free leading edge axial flow configuration. The plate will not undergo the second *in-vacuo* mode shape since divergence already occurs in the first mode shape. Since the three-dimensional twisting mode shape occurs at the third mode, it also will be adequate to use the beam model for the free leading edge configuration.

For comparison purposes, the first natural frequency based on the numerical analyses are shown in Table 1 and compared with the result of the analytical and experimental methods.

3.3. Experimental modal analysis

Experimental modal analysis was conducted to verify the results of analytical and numerical modal analyses. Plates will vibrate at different modes depending on the initial excitation force given during the experiment. The mode shape of interest in this study was the first mode shape since flutter would occur in the first mode shape in the configuration observed. To obtain the first mode shape for the *in-vacuo* experimental analysis it is enough to give an initial displacement to the tip of the plate. In this experiment, modal analyses were done by providing initial displacements for the plates and then allowing them to undergo free vibration. At the same time, the plates' responses to the initial conditions were recorded with a high-speed camera. The natural frequencies of all plates were calculated based on the extraction of images such as that shown in Fig. 3 and the results are presented in Table 1.

Fig. 3. Several frames of the experimental *in-vacuo* plate vibration test results using high speed camera.

Table 1 shows a comparison of the natural frequencies of the plates obtained with the three different methods. All three methods showed good agreement in terms of the first natural frequencies. In addition to the fact that the beam model has been validated by a three-dimensional finite element method, the experiment

also verified that both the beam model and the finite element method are representative of real plates.

4. Fluid Structure Interaction

Both numerical and experimental FSI analyses were executed in this research. Numerical simulations were intended to provide the flow visualization around the plates, while the experiments were done to verify the numerical simulations as well as to provide vibration characteristics of the plates as a function of air speeds.

4.1. Computational fluid structure interaction

The computational FSI simulation executed in this research was a time marching analysis using the interaction between the ANSYS STUDENT transient structural and the ANSYS STUDENT CFX (in a transient analysis setting). This FSI simulation solved equation (1) in the time domain. The analysis used the capability provided by the ANSYS finite element computer program in STUDENT version. ANSYS STUDENT has a transient structural sub-program that has the capability to solve transient structural deflections when given certain forces. ANSYS STUDENT also has a Computational Fluid Dynamics (CFD) sub-program to solve the fluid problem. In this study, the sub-programs were coupled to solve the free leading edge FSI configuration. In this time marching analysis, the deflection of the plates was solved at every time step using the ANSYS STUDENT transient structural sub-program. The ANSYS STUDENT CFX sub-program provided the aerodynamic force F_a as an input to the ANSYS STUDENT transient structural sub-program. The force F_a was calculated at each time step by this CFD sub-program.

An example of the simulation results is shown in Fig. 4, which is a plot of the total mesh displacement at each time step. CFX post-processing produced animated movement of the plate in the desired range of simulation times. As an example, Fig. 5 is a snapshot of the animation simulation results with the velocity vector field for a specimen with a thickness of 60 microns, width of 1 cm, and a length of 6 cm in air with a velocity of 12 m/s, which is the phase speed of the transition from an intermittent vibration pattern to the LCO vibration pattern.

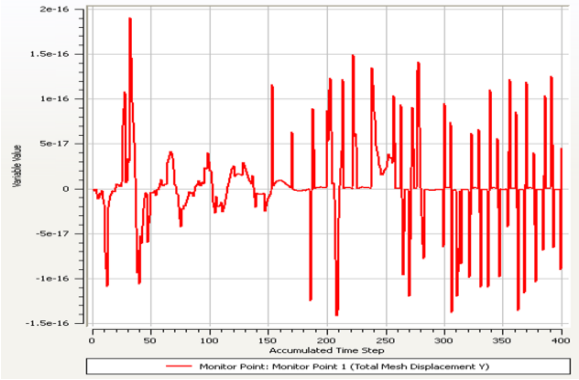

Fig. 4. A plot of total mesh displacement in accumulated time step.

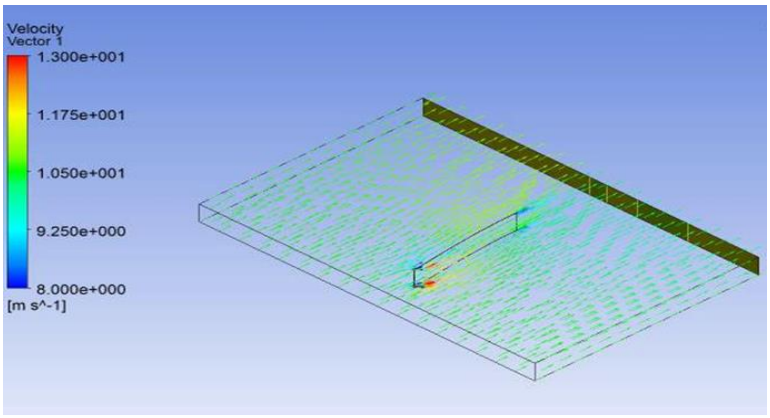

Fig. 5. A snapshot of the animation simulation results with the velocity vector field.

The post-processing of the result of this CFD simulation provided the flow visualization around the plate. This flow visualization was the tool that was used in explaining certain phenomena found in the free leading edge configuration such as the bistability, the intermittent vibration, LCO, and flutter. As shown in Fig. 5, there is a relative increase in the local air velocity at the tip of the free leading edge on the side on which the plate is deflected. A relatively higher air velocity means a lower air pressure. This implies that, as the CFD result suggests, there is an aerodynamic force acting on the plate on the side on which the plate is deflected. The bigger the plate deflection is, the higher the relative air velocity increases. This means that the aerodynamic force provides a negative stiffness. Also, it has been observed that the higher the air flow rate, the higher the increase in relative local air velocity. This means that as the air flow increases, the absolute value of aerodynamic stiffness also increases.

4.2. Experimental fluid structure interaction

Experiments were performed at Brawijaya University Wind Tunnel with a maximum speed of 40 m/s. In addition to five specimens that were presented in the modal analysis, five more plates were added in the FSI analysis to get a better picture of the data trends. These five extra plates were copper plates with the same aspect ratio of 1:6 and with three thicknesses of 60, 80, and 130 microns but different dimensions. The plates with the values of thickness of 60 and 80 microns have dimensions of 1.2 cm × 7.2 cm and 1.8 cm × 10.8 cm. The plate with the value of thickness of 130 microns has dimensions of 1.8 cm × 10.8 cm. So there were ten plates observed for FSI analysis. Note that the plate with a thickness of 130 microns and dimensions of 1.2 cm × 7.2 cm was excluded from the observations since it was found to have a flutter speed higher than the maximum speed of the wind tunnel being used.

Figure 6(a) is a photo of the actual experimental setup and Fig. 6(b) is the schematic experimental data acquisition setup. In one round of measurements, a single plate was placed in the wind tunnel. The air source came from a blower

that was run by an AC motor. The air speed was set by adjusting the intake valve. The wind tunnel was equipped with a honeycomb to obtain a smooth uniform laminar air flow. Wind speeds were measured using a pitot tube that was based on the difference between the air stagnation pressure and the static pressure. The observation was started with zero wind speed, continued by increasing the air speed, and ended when the post-critical flutter speed was obtained. The vibration characteristics of the plates were observed for all speed zones and recorded using a high-speed camera. This procedure was repeated for every plate.

The flutter speed for each plate was recorded along with its corresponding LCO speed. Table 2 shows the results of the experimental measurements of the flutter speeds for all plates. The LCO speeds tabulated here are the speeds where the plates start to show LCO. Figure 7 is a graph of the LCO and flutter speeds of all the plates. It can be generalized from this graph that a thicker plate with the same dimensions will have higher LCO and flutter speeds. Also, a wider or longer plate with the same thickness will have a lower LCO and flutter speed.

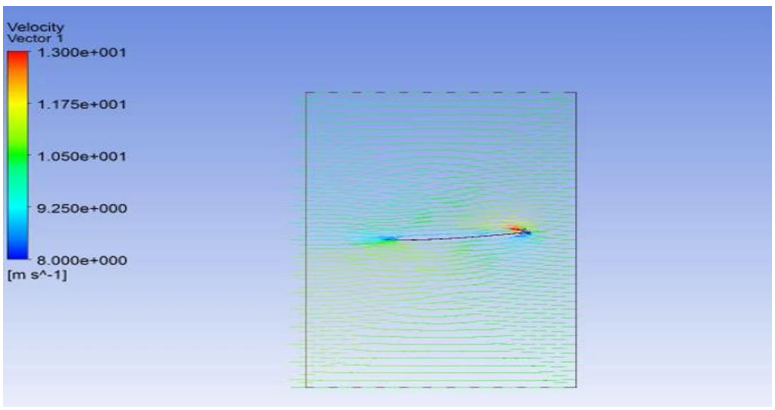

Table 2. The experimental flutter speeds of the plates with their corresponding subcritical LCO air speed.

Plate dimension	Air speed (m/s)	
	Subcritical LCO	Flutter
60 microns × 1 cm × 6 cm	8.36	11.71
80 microns × 1 cm × 6 cm	16.72	25.09
60microns × 1.2 cm × 7.2 cm	5.02	6.69
s80 microns × 1.2 cm × 7.2 cm	9.20	11.71
60 microns × 1.5 cm × 9 cm	3.34	4.52
80 microns × 1.5 cm × 9 cm	6.69	9.20
130 microns × 1.5 cm × 9 cm	25.09	35.12
60 microns × 1.8 cm × 10.8 cm	2.51	3.34
80 microns × 1.8 cm × 10.8 cm	3.34	4.52
130 microns × 1.8 cm × 10.8 cm	11.71	18.40

(a)

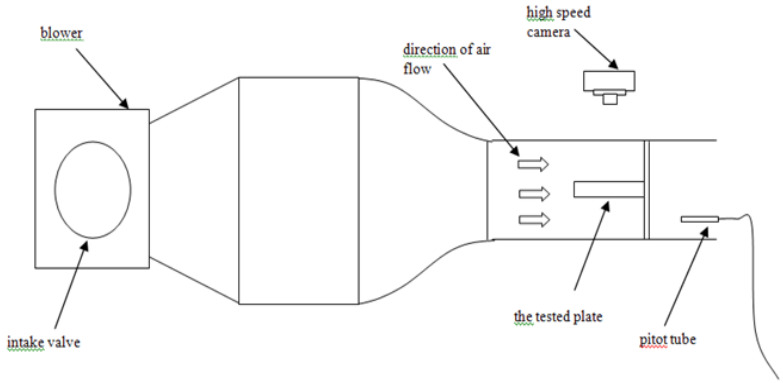

(b)

Fig. 6. (a) The photo of the experimental setup and (b) the schematic of the experimental setup.

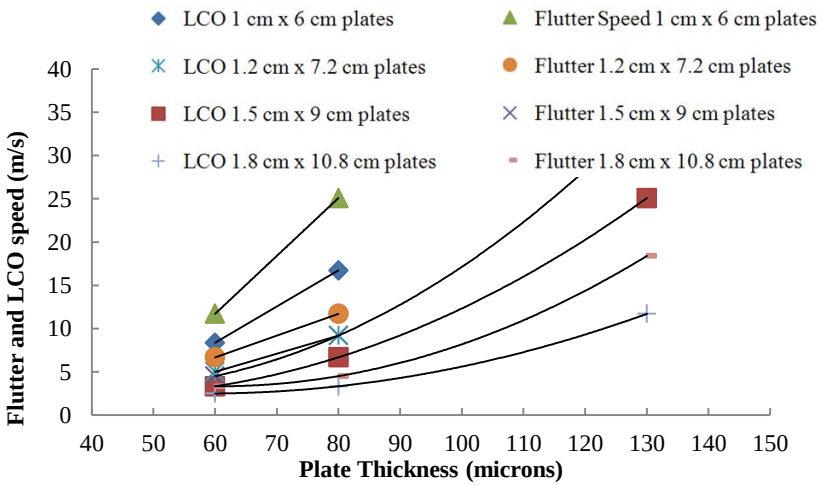

Fig. 7. The flutter speeds of the plates and the speed when the plates reach the sub critical LCO.

The experimental observations showed that the vibration characteristics of the plates change with speed. There are four speed zones based on the vibration

characteristics of the plates. The vibration behaviors of the plates were observed using a high-speed camera in every speed zone. Several videos were taken by the high-speed camera with 210 frames-per-second camera speed. Then, the recorded videos were extracted to obtain the frame-by-frame plate movements as for example shown in Fig. 8. These frame-by-frame pictures were used to generate the phase plane diagrams, as shown in Fig. 9, and to measure the amplitudes of the plate deflections when they experienced the LCO, as shown in Fig. 10.

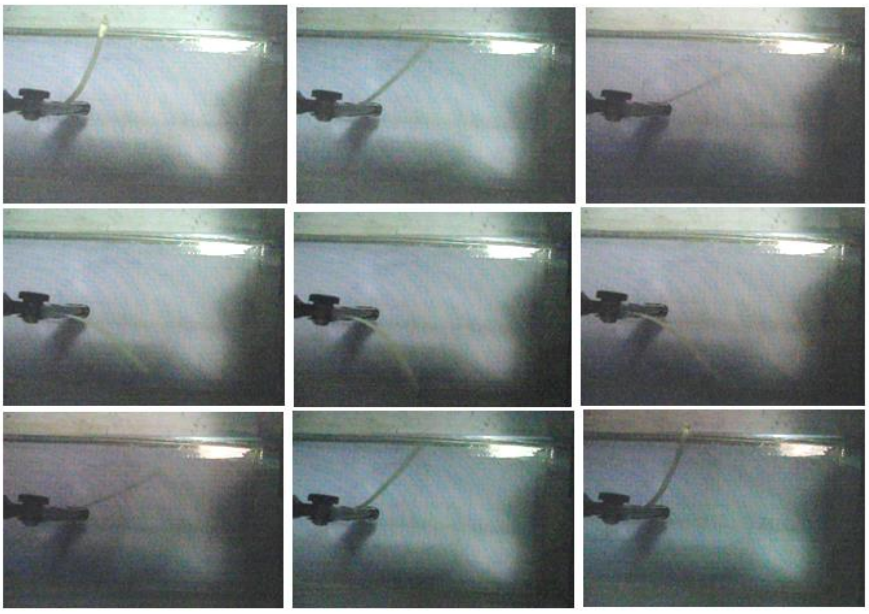

Fig. 8. The plate exhibited a nearly periodic LCO at a certain speed below the flutter speed. The pictures were taken with the plate's dimension of 60 microns x 1 cm x 6 cm.

The experimental observations showed that the vibration characteristics of the plates changed with speed. There were four speed zones observed for the vibration characteristics of the plates:

i. Stand still/hardly move

When the air speed was slowly raised from zero, the plates were still or hardly moving. In this speed zone, the plate movements were hardly noticeable or on occasion they deflected slightly and returned back to the original equilibrium position. The phase plane diagram in Fig. 9(a) is an example of the plate's behavior in this speed zone.

ii. Intermittent vibration

More frequent and bigger plate deflections occur as the wind speed increased. The plates returned back to the original position after they oscillated by one or more cycles. The plates stood still for a while before deflecting again. See Fig. 9(b). Whenever the curve reached the origin of the phase plane the plate rested for a while in the initial position. There was no certain periodic deflection observed in

this speed zone. The intermittent deflections occurred in a seemingly random manner. There has been no intermittent vibration reported in previous studies of fixed leading-edge plates by other researchers. The intermittent vibration leads to the free leading-edge axial flow configuration.

The presence of the intermittent vibrations here could be predicted due to the nature of the bistable equilibrium of a counter axial flow. Recall the bistable analysis that has been discussed in section 2. Qualitatively, using static aeroelastic analysis, in the first mode shape, the plate has two stable equilibrium positions on both sides of the original position and the original equilibrium position becomes unstable. As the air speed increases, the value of aerodynamic stiffness K_a increases. This means that the two new stable equilibrium positions move away from the original equilibrium as the air speed increases. The numerical FSI simulation also showed the existence of an intermittent vibration, as shown in Fig. 4.

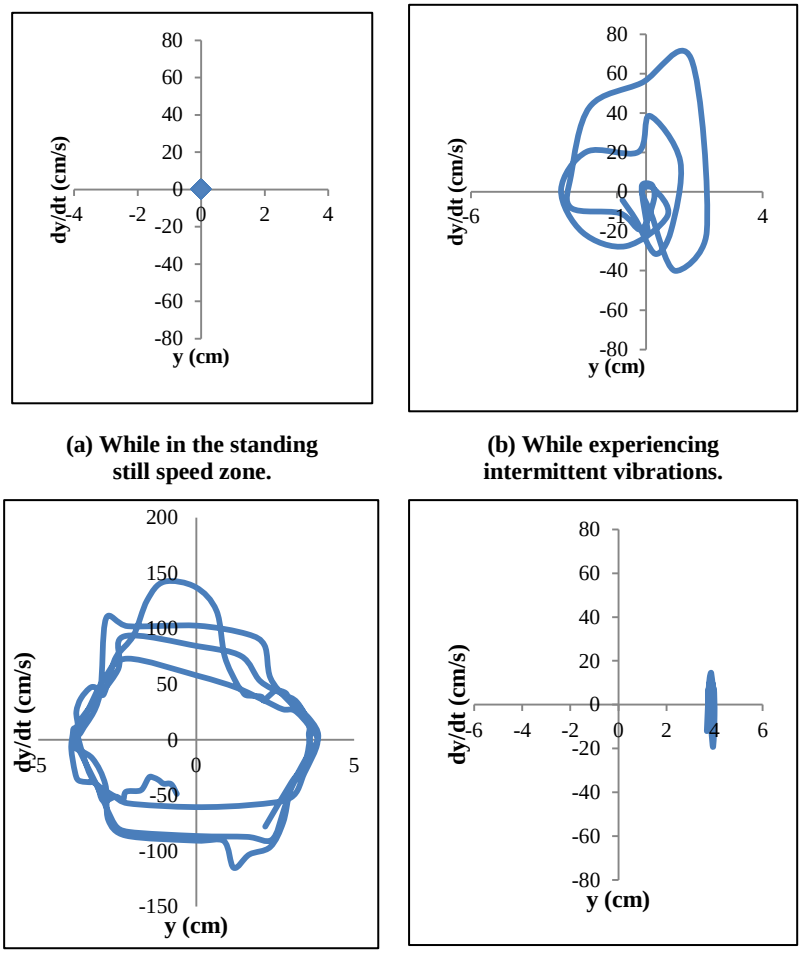

(a) While in the standing still speed zone.

(b) While experiencing intermittent vibrations.

(c) While experiencing subcritical LCO.

(d) While experiencing post-critical flutter.

Fig. 9. Phase plane of the deflection of tip of the leading edge the plate.

The aerodynamic stiffness K_a is the linearized coefficient of the aerodynamic force acting on the plate with respect to the displacement matrix. This aerodynamic force is nonlinear in nature. This nonlinearity contributes to the seemingly random behavior of the observed intermittent vibrations.

iii. Subcritical LCO

When the air speed was raised further and left the intermittent vibration zone, the new two stable equilibriums moved further outwards and the condition of a subcritical LCO was achieved. As the air speed increased further, a nearly periodic LCO occurred in this speed zone before the plates experienced flutter. Fig. 9(c) shows that the phase plane never passed through the origin in this case. This means that a continuous vibration occurred in this speed zone. The variation of the maximum speed indicates that the period of the oscillation was not constant. Although the period of oscillations was not constant, the period of LCO of a certain plate approached a certain average value. The variations of the periods of the oscillations indicate the nonlinearity of the aerodynamic force.

iv. Post-critical speed

As the bistable equilibrium positions moved further outwards with the increase in air speed, divergence was reached. The plate deflected outward and did not return back to the original position. The air speed when this unstable condition occurs is known as the flutter speed. When the air speed was increased further from this critical condition, the post-critical condition was achieved (see Fig. 9 (d)).

For generalization, the mapping of plate vibration characteristics for every speed zone was done using a normalized plot, as shown on Fig. 10. This graph is the plot of the normalized amplitudes as a function of the normalized speeds. The normalized amplitudes Y are the ratios of the amplitudes of the plates free leading edge y and the plates' length L.

$$Y = \frac{y}{L} \tag{11}$$

The normalized speeds V_{norm} are the ratios of the air speeds V and the experimental plates flutter speeds V_f.

$$V_{norm} = \frac{V}{V_f} \tag{12}$$

The normalized amplitudes of the plates during the LCO vibrations that were measured from the experiments are plotted in this graph. The diamonds are the normalized amplitudes of the subcritical LCO from the experimental data and the trend line is the approximation of the normalized amplitudes of the plates for all speed zones. Based on the experiments, the standing still zone ranges from 0 to 0.2 normalized speeds; the intermittent vibration zone ranges from 0.2 to 0.6; the subcritical LCO vibration zone ranges from 0.6 to 1; and the post-critical vibration zone ranges from 1 upwards.

The experimental observations regarding the vibration characteristics provide insight to the utilization of the free leading edge axial flow configuration for wind harvesting. The suitable speed zones for wind harvesting range from the

intermittent to the subcritical LCO zones, with the optimum condition in the latter. The experiments also showed that a stiffer plate (which also means having a higher natural frequency) has a higher flutter speed. This means that a less stiff plate is more appropriate to lower wind speeds. The experiments prove that the free leading edge axial flow configuration experienced flutter in its first mode shape, which means that flutter could occur at lower wind speeds compared to the axial flow case. Due to the nature of the flutter mode shape, the appropriate placement of the piezoelectric electrical energy converter is at the fixed downstream edge.

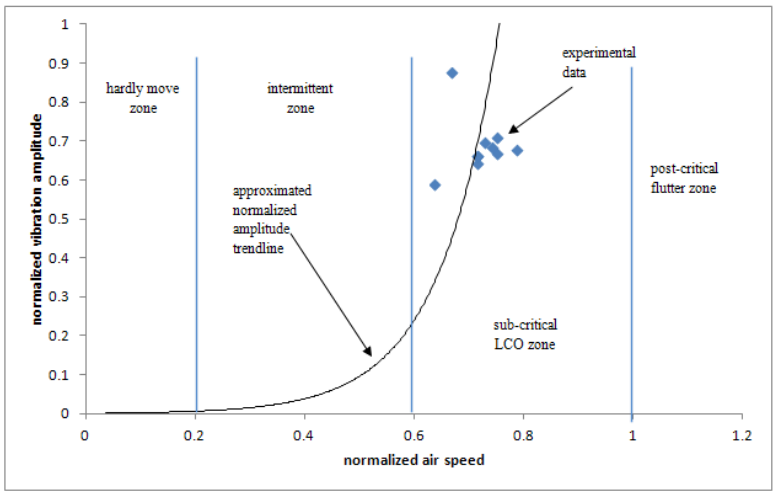

Fig. 10. Normalized speed zones.

5. Conclusions

Aeroelastic behavior of cantilevered thin flat plates with a free leading edge in an axial flow air stream have been described in this article such that flutter occurs in the first mode shape of the *in-vacuo* modal analysis results. The numerical and experimental results of this study provide some insight for the utilization of this configuration as a new alternative for wind harvesting with the advantages that flutter could occur at a lower mode shape that would be more appropriate for lower wind speeds. Wind speed zones that can be used for wind harvesting range from the beginning of the intermittent vibration zone until the subcritical LCO speed zone, with the optimum conditions achieved in the subcritical LCO zone.

A new finding has been introduced by the present study in the form of the intermittent vibration phenomenon that is unique to the free leading edge axial flow plate configuration. It is concluded that the intermittent vibration phenomenon leads to the free leading edge plate configuration due to its bistable nature.

The current research is a classical flutter analysis. Future work could extend this research toward stall flutter analysis with non-zero angle of attack to investigate the opportunities for obtaining a better wind harvesting configuration.

References

1. Deivasigamani, A.; McCarthy, J.M.; John, S.; Watkins, S.; Trivailo, P.; and Coman, F. (2013). Flutter of cantilevered interconnected beams with variable hinge positions. *Journal of Fluids and Structures*, 38, 223-237.
2. Rayleigh, Lord. (1978). On the instability of jets. *Proceedings of the London Mathematical Society*, 10, 4-13.
3. Theodorsen, T. (1935). General theory of aerodynamic instability and the mechanism of flutter. *National Advisory Committee for Aeronautics' Technical Report* No. 496.
4. Theodorsen, T.; and Garrick, I.E. (1940). Mechanism of flutter: theoretical and experimental investigation of the flutter problem. *National Advisory Committee for Aeronautics' Technical Report* No. 685.
5. Theodorsen, T.; and Garrick, I.E. (1941). Nonstationary flow about wing-aileron-tab combination including aerodynamic balance. *National Advisory Committee for Aeronautics' Technical Report* No. 736.
6. Watanabe, Y.; Isogai, K.; Suzuki, S.; and Sugihara, M. (2002). A theoretical study of paper flutter. *Journal of Fluids and Structures*, 16, 543-560.
7. Watanabe, Y.; Suzuki, S.; Sugihara, M.; and Sueoka, Y. (2002). An experimental study of paper flutter. *Journal of Fluids and Structures*, 16, 529-542.
8. Connell, B.S.H.; and Yue,D.K.P. (2007). Flapping dynamics of a flag in a uniform stream. *Journal of Fluid Mechanics*, 581, 33-67.
9. Lemaitre, C.; Hémon, P.; and deLangre, E. (2005). Instability of a long ribbon hanging in axial air flow. *Journal of Fluids and Structures*, 20(7), 913-925.
10. Michelin, S.; Smith, S. G. L.; and Glover, B.J. (2008). Vortex shedding model of a flapping flag. *Journal of Fluid Mechanics*, 617, 1-10.
11. Manela, A.; and Howe, M.S. (2009). On the stability and sound of an unforced flag. *Journal of Sound and Vibration*, 321,994-1006.
12. Virot, E.; Amandolese, X.; and Hémona, P. (2013). Fluttering flags: An experimental study of fluid forces. *Journal of Fluids and Structures*, 43,385-401.
13. Gibbs, S. C.; Wang, Ivan; and Dowell, Earl (2012). Theory and experiment of a rectangular plate with fixed leading edge in three-dimensional axial flow. *Journal of Fluids and Structures*, 34, 68-83.
14. Tang, D.; and Dowell, E. (2002). Limit cycle oscillations of two-dimensional panels in low subsonic flow. *International Journal of Non-linear Mechanics* 37(7), 1199-1209.
15. Tang, D.; Yamamoto, H.; and Dowell, E. (2003). Flutter and limit cycle oscillations of two-dimensional panels in three-dimensional axial flow. *Journal of Fluids and Structures* 17, 225-242.
16. Tang, Liaosha; and Païdoussis, M.P. (2009). The coupled dynamics of two cantilevered flexible plates in axial flow. *Journal of Sound and Vibration*, 323, 790-801.
17. Zhao, Wensheng; Païdoussis, M.P.; Tang, Liaosha; Liu, Meiqing; and Jiang, Jin. (2012). Theoretical and experimental investigations of the dynamics of

cantilevered flexible plates subjected to axial flow. *Journal of Sound and Vibration*, 331, 575-587.

18. Howell, R.M.; Lucey, A.D.; Carpenter, P.W.; and Pitman, M.W. (2009). Interaction between a cantilevered-free flexible plate and ideal flow. *Journal of Fluids and Structures*, 25, 544-566.
19. Howell, R.M.; Lucey, A.D.; and Pitman, M.W. (2011). The effect of inertial in homogeneity on the flutter of a cantilevered flexible plate. *Journal of Fluids and Structures*, 27, 383-393.
20. Doaré , O.; Sauzade, M.; and Eloy, C. (2011). Flutter of an elastic plate in a channel flow: confinement and finite-size effects. *Journal of Fluids and Structures*, 27, 76-88.
21. Huang, Lixi; and Zhang, Chao. (2013). Modal analysis of cantilever plate flutter. *Journal of Fluids and Structures*, 38,273-289.
22. Eloy, C.; Souilliez, C.; and Schouveiler, L. (2007). Flutter of a rectangular plate. *Journal of Fluids and Structures*, 23(6), 904-919.
23. Eloy, C.; Lagrange, R.; Souilliez, C.; and Schouveiler, L. (2008). Aeroelastic instability of cantilevered flexible plates in uniform flow. *Journal of Fluid Mechanics*, 611, 97-106.
24. Eloy, C.; Kofman, N.; and Schouveiler, L. (2012). The origin of hysteresis in the flag instability. *Journal of Fluid Mechanics*, 691, 583-593.
25. Drazumeric, R.; Gjerek, B.; Kosel, F.; and Marzocca, P. (2014). On bimodal flutter behavior of a flexible airfoil. *Journal of Fluids and Structures*, 45, 164-179.
26. Balint, T.; and Lucey, A. (2005). Instability of a cantilevered flexible plate in viscous channel flow. *Journal of Fluids and Structures* 20, 893-912.
27. Huang, L. (1995). Flutter of cantilevered plates in axial flow. *Journal of Fluids and Structures*, 9(2), 127-147.
28. Doaré, O.; and Michelin, S. (2011). Piezoelectric coupling in energy-harvesting fluttering flexible plates: linear stability analysis and conversion efficiency. *Journal of Fluids and Structures*, 27, 1357-1375.
29. Dunnmon, J.; Stanton, S.; Mann, B.; and Dowell, E. (2011). Power extraction from aeroelastic limit cycle oscillations. *Journal of Fluids and Structures*, 27, 1182-1198.
30. Allen, J.J.; and Smits, A.J. (2001). Energy harvesting eel. *Journal of Fluids and Structures*, 15(3-4), 629-640.
31. Kuhl, J.M.; and DesJardin, P.E. (2012). Power production locality of bluff body flutter mills using fully coupled 2D direct numerical simulation. *Journal of Fluids and Structures*, 28, 456-472.
32. Howell, R.M.; and Lucey, A.D. (2015). Flutter of spring-mounted flexible plates in uniform flow. *Journal of Fluids and Structures*, 59, 370-393.
33. Meijer, Marius-Corné; and Dala, Laurent. (2015). Zeroth-order flutter prediction for cantilevered plates in supersonic flow. *Journal of Fluids and Structures*, 57, 196-205.
34. Fernandes, A.C.; and Mirzaeisefat, S. (2015). Flow induced fluttering of a hinged vertical flat plate. *Ocean Engineering*, 95, 134-142.

35. Cunha-Filho, A.G.; de Lima, A.M.G.; Donadon, M.V.; and Leão, L.S. (2016). Flutter suppression of plates using passive constrained viscoelastic layers. *Mechanical Systems and Signal Processing*, 79, 99-111.
36. Darbandi, Masoud; and Fouladi, Nematollah (2016). Numerical study of flow-induced oscillations of two rigid plates elastically hinged at the two ends of a stationary plate in a cross-flow. *Journal of Fluids and Structures*, 66, 147-169.
37. Tubaldi, E.; Amabili, M.; and Alijani, F. (2015). Nonlinear vibrations of plates in axial pulsating flow. *Journal of Fluids and Structures*, 56, 33-55.
38. Akaydin, H.D.; Elvin, N.; and Andreopoulis, Y. (2010). Energy harvesting from highly unsteady fluid flows using piezoelectric materials. *Journal of Intelligent Material Systems and Structures*, 21, 1263-1278.
39. Inman, D.J. (1994). *Engineering vibration.* New Jersey: Prentice-Hall, Inc.